EFFICIENCY OF DIFFERENT MACHINE LEARNING METHODS FOR SHORELINE EXTRACTION FROM UAV IMAGES

Bulent Bayram (1), Dursun Zafer Seker (2), Burak Akpinar (1)

[1] Yildiz Technical University, Department of Geomatics Engineering, Davutpasa Campus, Esenler, 34220, Istanbul-Turkey
[2] Istanbul Technical University, Department of Geomatics Engineering, 80626 Maslak Istanbul, Turkey
Email: bayram@yildiz.edu.tr; seker@itu.edu.tr; bakpinar@yildiz.edu.tr

KEY WORDS: Support Vector Machines, Random Forest, water body classification, shoreline extraction, UAV

ABSTRACT: Shorelines are valuable assets of coastal areas that possess unique features. A huge user community is associated with the shorelines, which may be affected by both natural and human-induced factors. Monitoring of such areas is crucial for environmental protection, sustainable development and planning. Shoreline extraction is a fundamental step to determine their dynamics that is crucial for conservation of various natural habitats. The recent developments in Unmanned Aerial Vehicle (UAV) systems have made it possible to acquire high-resolution images at low cost, which can be exploited for shoreline mapping. This study aims to investigate the efficiency of Support Vector Machines (SVM) and Random Forest (RF) classifiers to obtain accurate and reliable water body and land classes from a very high-resolution digital orthophoto achieved using UAV-images. In the study, a 3.3 km shoreline located on the Black Sea coastline was selected as the study area. The digital orthophoto was generated using commercial software based on the SfM method with 1.96 cm ground sample distance. The SVM and RF methods were used to achieve land, water body and wave classes to generate the shoreline of the study area. The same training data were used for both the SVM and RF methods. Rapid illumination changes during flights caused unbalanced color on the entire image. Considering this effect, nine patches were created from the orthophoto image. Each patch was handled as an individual image and training samples had to be selected for each class from each patch.

The shorelines have been generated from binary water body and land classes. Accuracy ssessment was performed by comparing results with Global Navigation Satellite System (GNSS) measurements. The average errors were calculated as 0.935 m and 0.939 m for the SVM and RF methods, respectively. The differences of 71.86% and 71.61% are in the 0–1 m interval for SVM and RF, respectively.

Although the SVM and RF methods have been used in various studies for image classification purposes, they have not been utilized for shoreline extraction. This study shows that these two machine-learning methods also provide remarkable results for this purpose. The proposed framework can be used to create an essential data source for many coastal-related studies such as monitoring, determining temporal changes and modelling sediment transport.

This study has been supported by TUBITAK (The Scientific and Technological Research Council of Turkey) with project number 115Y718.

1. INTRODUCTION

Accurate and high-resolution data for monitoring and defining coastal changes are vital for coastal management. Even though there are many conventional techniques used for data collection, recently UAVs and photogrammetric evaluation of the obtained images have become very popular among coastal researchers, administrators and decision makers. The advantages of Structure from Motion (SfM) photogrammetry and the increasing capacity of computer systems have opened new perspectives for the generation of three-dimensional point cloud and digital orthophotos (Clapuyt et al., 2016). Accordingly, UAVs have become an essential tool for coastal monitoring in local areas due to their cost-effectiveness and ease of use (Clark, 2017). Therefore, many researchers have focused on the use of UAVs in various coastal-related studies.

Oleire-Oltmanns (2012) used UAVs for erosion monitoring of a coastal area from generated orthophotos and a digital elevation model (DEM) using stereoscopic digitizing and DEM analysis. Flener et al. (2013) used mobile LiDAR,

UAV photography and optical bathymetric modelling to map river channels. Mancini et al. (2013) used UAV for reconstruction of coastal environments. They validated UAV-SfM and Terrestrial Laser Scanning (TLS) results with GNSS measurements. Casella et al. (2014) determined beach topography using UAV-derived orthophotos and DEM with commercial geographical information system (GIS) software. Mišijovský et al. (2015) used a UAV system to monitor changes at the Morava River near Litovel. They determined the changes by historical maps and orthophoto images generated from UAV images and compared transversal profiles. Lim et al. (2015) exploited UAV to measure the effects of organic carbon bearing at coastal dune cliffs. They used UAV survey differences, TLS and pseudo three-dimensional ground-penetrating radar (GPR). Čermáková et al. (2016) utilized UAV for detection of changes to shorelines. The shorelines were manually digitized from orthophoto images created by the SfM method using UAV images. Kalke and Loewen's (2018) study determined the ice conditions of the North Saskatchewan River and the Peace River using UAV and bridge-mounted game camera images. They used the SVM method to obtain ice surface and water classes from UAV images. Bayram et al. (2017) applied an object-based fuzzy segmentation method to extract shoreline from UAV-derived orthophoto images. Scarelli et al. (2017) used UAVs to define seasonal changes to the dunes and beach on the Ravenna coast, Italy, by employing a surface comparison based method. Rusnák et al. (2018) also used UAV technology for river landscape mapping. They utilized supervised maximum likelihood to obtain water area, bar surface, vegetation woody debris and bare surface classes from digital orthophotos. Talavera et al. (2018) detected morphodynamic changes at Camposoto beach (SW Spain) by the DEM of Difference method from UAV-derived orthophotos. Noleta et al. (2018) presented a framework for monitoring coastal dune development using a multispectral UAV system based on the k-means clustering method. Milas et al. (2018) compared maximum likelihood and SVM classifiers to create land cover/classes from UAV-derived orthophoto images from the Old Woman Creek National Estuarine Research Reserve in Ohio, USA. Guillot et al. (2018) proposed a method to compute the volume of a coastal dune from UAV images using an adapted version of the "cut and fill" method. Xia et al. (2018) proposed a method for mapping wetland inundation. They combined UAV and Landsat-8 Operational Land Imager (OLI) data. To create a UAV land cover map, they used an object-based image classification method. They used linear spectral unmixing, artificial neural networks and regression tree methods to create a subpixel inundation map. Mallast and Siebert (2019) investigated submarine groundwater discharge by UAV-based thermal infrared measurements. Nagarajan et al. (2019) used a UAV system to determine the shoreline retreat at the Jupiter Inlet Lighthouse ONA caused by Hurricane Irma. They manually digitized shorelines from pre- and post-hurricane orthomosaic images. Spatial change detection was determined by transect-based analysis.

Water body segmentation issues are a primary step in shoreline extraction. Coastal image segmentation is of vital importance in extracting shorelines. Various pixel- and object-based image segmentation methods from aerial orthophoto and satellite imageries have been proposed. Geostatistical methods, spatial attraction models, Artificial Neural Networks (ANN), Wavelet Transform, Genetic Algorithms, Markov Random Field and RF Mean-Shift integrated fuzzy clustering methods can be given as some examples (Demir et al., 2017, 2019; Liu et al., 2016). More information can be found in Zaitoun and Aqel (2015).

The objective of this study is to test two well-known machine learning algorithms (SVM and RF) for extraction of shorelines from high-resolution digital orthophotos obtained from UAV-derived images. The impression obtained from the literature review is that these methods were not previously employed for shoreline extraction by using high-resolution data; thus this study aims to eliminate this gap in the literature. The results were then compared with GNSS measurement to evaluate performance. In this study, we propose a UAV-based framework by exploiting two machine learning methods for shoreline extraction, which has indispensable importance for detecting temporal change, coastal preservation and rapid and cost-effective monitoring of erosion and natural hazard effects, focusing on coastal areas.

2. STUDY AREA

The selected study area comprises the 3.3-km shoreline of Istanbul-Terkos Lake located on the Black Sea coastline between the Terkos Lake Dam Basin (built in 1883) and the Karaburun-Ormanlı region. Erosion in the region causes significant dune loss and damage (Figure 1). Natural and anthropogenic effects are the main threats of erosion. For example, sand mining is one the main reason of erosion that also causes depletion of resources, deterioration of

coastal structures and damages fish nests.

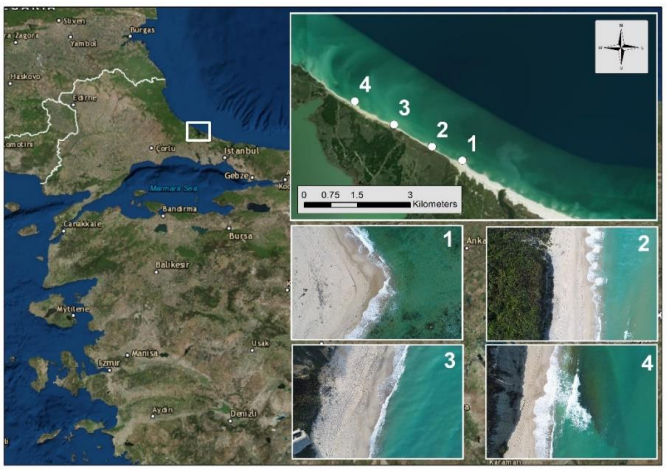

Figure 1 Study area

3. MATERIALS AND METHODS

This study consists of three main steps: orthophoto generation, SVM and RF implementation, and accuracy assessment. The flowchart of the study is given in Figure 2. Digital orthophotos are the building blocks of the proposed framework. First of all, UAV images were captured by the Multirotor G4 Eagle V2 UAV system with a Sony Alpha 7R camera (36.4 MP 35mm Full-Frame Exmor® CMOS Sensor, Sony SEL 35mm f/2.8 ZA Carl Zeiss Lens) on 20 September 2017. The flight height was 70 m and endlap and sidelap overlaps were 80% and 70%, respectively. The study area was covered with two columns and the total number of captured images was 372. Since the precision of the inertial measurement unit (IMU) and GPS systems was low, 25 ground control points were measured using the real-time kinematic (RTK) GNSS method as well as the reference shoreline.

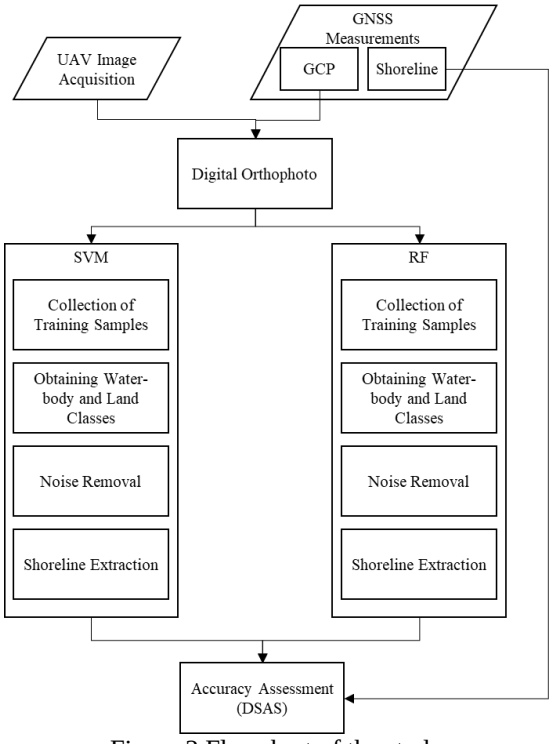

Figure 2 Flowchart of the study

3.1. Digital orthophoto generation

3D point cloud and digital orthophotos of the study area were created by commercial Pix4d software (Pix4d, 2017), which is based on the SfM technique. Although this method was developed in 1979 (Ullman, 1979), due to rapid developments in computers/workstations and camera systems, SfM photogrammetry became an indispensable tool

for creating 3D point cloud and digital orthophotos from UAV images (Gomez et al., 2015). SfM photogrammetry has been implemented in many different studies. The details of the SfM algorithm can be found in Murtiyoso and Pierre (2017) and Dellaert et al. (2000).

3.2.Machine learning based classification

In this study, two different machine learning algorithms have been utilized for shoreline extraction. Due to their proven image classification performance, both the SVM and RF methods were chosen to create water body and land classes from digital orthophotos.

3.3.Support Vector Machines

SVM is a machine-learning based method developed by Vapnik (1995). The method is based on statistical learning and structural risk minimization from training samples. Training samples are used to construct decision functions which are called support vectors. The hyperplane is defined by using support vectors. The optimum hyper plane is defined by decision function (Vapnik, 1999).

The support vector machines have had a significant impact on classification of complex patterns. SVMs have been widely used in various applications due to their effectiveness even with a small sample size for training (Gu et al., 2016). The objective in such a case is to find an optimal hyperplane between the two classes such that it maximizes the margin of separation between them. According to Haykin (2009), the details of the method are given as follows:

Consider a binary classification problem with two linearly separable classes. Let $\{X_i , Y_i\}_{i=1}^{N}$ represent training samples, where N is the number of training examples and Yi ={-1 , +1} are target values of respective classes. We can find an optimal hyperplane that maximizes the distance between two classes which can be represented as in equation (1):

$$W^T X + b = 0 \tag{1}$$

Here X is the input vector, W is the weight vector and b is bias, Yi=+1 represents the positive class and Yi =-1 represents the negative class. In order to find the optimal hyperplane, the parameters W and b should be estimated in such a way that they satisfy equations (2) and (3):

$$W^T X_i + b \geq +1 \qquad \text{for Yi =+1} \tag{2}$$
$$W^T x_i + b \leq -1 \qquad \text{for Yi = -1} \tag{3}$$

Geometrically, the distance between the closest data point and the hyperplane is called the margin. The margin between the two classes can then be obtained as in (4):

$$\text{Margin} = \left(\frac{2}{||w||}\right) \tag{4}$$

Hence, to maximize the margin of separation between the two classes, the factor $\frac{2}{||W||}$ needs to be maximized. For mathematical convenience it is sometimes rewritten as $\frac{1}{2}\ ||w||^{2}$. To find an optimal hyperplane, the Euclidean norm of the weight vector needs to be minimized.

The solution to the optimization problem can be obtained by converting the constrained problem into a non-constrained problem by applying Lagrange multipliers:

$$L(w, x, \alpha) = \frac{1}{2} w^T w - \sum_{i=1}^{N} \alpha_i \{y_i (w^T x_i + b) - 1\} \tag{5}$$

where the variables α_i are called Lagrange multipliers and N is the number of training examples that corresponds to non-zero Lagrange multipliers called support vectors. Equation (5) needs to be minimized for the variables *w* and x:

$$L(w, x, \alpha) = \sum_{i=1}^{N} \alpha_i - \frac{1}{2} \sum_{i=1}^{N} \sum_{j=1}^{N} \alpha_i \alpha_j Y_i Y_j X^T{}_i X_j \tag{6}$$

To get the optimal solution for the dual problem, equation (6) needs to be maximized. For a linearly separable

classification problem, there is a global optimal solution under the given constraints. Naturally, not all problems are linearly separable and no feasible solution can be obtained as equation (6) cannot be applied directly to such complex problems. An alternate solution could be to transform the input data to a higher dimension by applying a kernel function. The transformed data are supposed to be linearly separable and the SVM classifier could introduce a hyperplane to separate the data. Equation (6) can be rewritten with a kernel function as equations (7) and (8):

$$L(\alpha) = \sum_{i=1}^{N} \alpha_i - \frac{1}{2} \sum_{i=1}^{N} \sum_{j=1}^{N} \alpha_i \alpha_j y_i y_j K(x_i, x_j) \quad (7)$$

$$\text{where } K(x_i, x_j) = \phi(x_i)\phi(x_j) \quad (8)$$

The K is called the kernel function. A number of options are available for kernel selection. However, for the purpose of this study the radial basis function (RBF) kernel is used as it has been successfully used in a number of classification tasks (Ghamisi et al., 2017). RBF can be expressed mathematically as:

$$K(x, x') = \exp\left(\frac{||x - x'||^2}{2\sigma^2}\right) \quad (9)$$

3.4.Random Forest

RF is an ensemble classifier that combines a number of individual tree predictors to form a powerful classification model. It is a useful method as significant improvements can be obtained in the classification accuracy by letting the individual trees vote for the most popular class. The generalization error of an RF classifier depends on the strength of the individual trees in the forest (Breiman, 2001).

RFs are trained to obtain an optimal number of trees. Usually two-thirds of the training samples are used to train the trees, while the remainder are used for cross-validation to estimate the performance of the RF model (Belgiu & Drăguţ, 2016). The user needs to define the number of decision trees (N) to be constructed. RF randomly grows the forest up to N with maximum variance and low bias. The final decision about a test sample is taken by averaging the resulting probabilities of individual trees. This means that the test data are evaluated by each tree in the ensemble and its membership is decided based on the maximum voting of the trees for a particular class.

A bootstrap sampling method is used for random selection. Tree development from selected attributes is done according to the CART algorithm. The CART algorithm uses the Gini index for best attribute selection (Breiman, 2001). The Gini index is a confusion-based method that calculates the differences between the probability distributions of the target attribute values. The Gini index is calculated for data set D (Han et al., 2011):

$$Gini(D) = 1 - \sum_{i=1}^{n} p_i^2 \quad (10)$$

pi is the probability of the ith class in D. The Gini index is based on a binary split for each attribute. In order to determine the best binary division A, all possible subsets are examined. For the attribute A, the D data set is divided into two subgroups as D1 and D2 and the Gini index is calculated according to equation (11):

$$Gini(D) = \left|\frac{D_1}{D}\right| Gini(D_1) + \left|\frac{D_2}{D}\right| Gini(D_2) \quad (11)$$

Possible binary splits of each attribute are considered. The point which gives the minimum Gini index is selected as the split point of that attribute.

The subset that provides the lowest Gini A (D) value is selected as the binary subset. This process is applied for each attribute. The class homogeneity can be measured by the Gini index.

According to Belgiu and Drăguţ (2016), the computational complexity of the RF for model construction can be predicted as follows:

$$\text{Time Complexity} = T\sqrt{(MxNx\log(N))} \quad (12)$$

where T is the number of random trees in RF, M represents the number of variables used in the split and N is the number of training examples.

RF classifier construction requires two parameters: the number of decision trees (N) and the number of variables used to split data (M). First, bootstrap samples are created from two-thirds of the training data set. The remaining one-third of the training set, called out-of-bag (OOB) data, is used to test for errors. The trees are developed without

pruning from each bootstrap sample. In each node, M variables are randomly selected among all variables and the best branch is determined between these variables. Generally, N has less impact on the classification accuracy of the classifier. Since increasing the value of N does not overfit the RF classifier, it can be as large as possible. The M is usually determined by taking the square root of the number of input variables (Gislason et al., 2006). Increasing the value of M may increase the computational time of the RF classifier as it has to compute the information using all the variables to split data. Also making the M equal to the number of features can reduce the performance as it will result in highly correlated trees. Therefore, a subset of the features k<M is selected to split the data (Jamil, 2018).

In this study, the number of trees and the random variable have been selected empirically.

4. RESULTS AND DISCUSSION

The digital orthophoto was generated using commercial software based on the SfM method with 1.96 cm ground sample distance. The adjustment results are given in Table 1.

Table 1 Adjustment results

	X	Y	Z
Mean (cm)	0.17	0.27	1.84
Sigma (cm)	1.85	2.00	7.77
RMS Error (cm)	1.86	2.02	7.98

The SVM and RF methods were used to achieve land, water body and wave classes to generate the shoreline of the study area. The same training data were used for both the SVM and RF methods. Rapid illumination changes during flights caused unbalanced colour on the entire image. Considering this effect, nine patches were created from the orthophoto image. Each patch was handled as an individual image and training samples had to be selected for each class from each patch. The generated digital orthophoto and a sample of colour differences between two patches are displayed in Figure 3. The total number of pixels for each patch and the patch- based total number of training pixels for each class are given in Table 2.

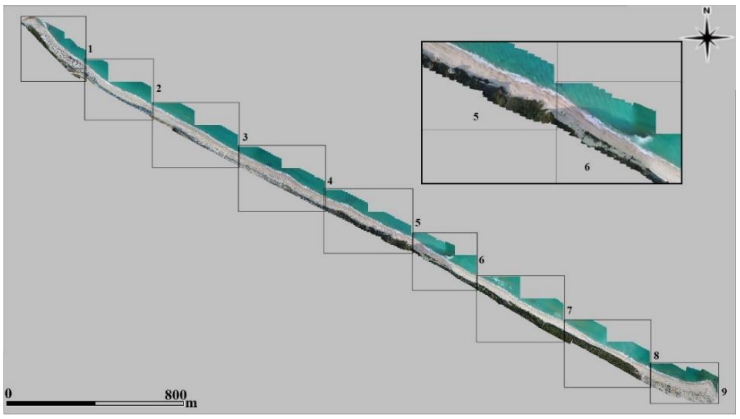

Figure 3 Generated digital orthophoto

Table 2 Measured training samples in each patch of orthophoto image

Patch No	Total number of pixels	The number of training pixels				
		Land	Water body	Wave	No Data	Total
1	226306820	11873	3313	12126	141	27453
2	224087300	13386	4815	6335	335	24871
3	301193935	4095	1617	6256	4440	16408
4	307558350	6643	7223	4816	2962	21644
5	306947815	5880	18888	8653	2320	35741
6	199635900	11146	30184	7284	1031	49645
7	311057916	15909	17731	5290	9753	48683
8	312706899	11153	18077	4964	1092	35286
9	149083272	18561	21081	9305	1737	50684

The kernel type, gamma and penalty parameters for SVM were Radial Basis Function, 0.250 and 100, respectively. The number of trees and random variable were set as 50 and 2 for the RF method.

The water body and wave classes merged as water body and another class as land to create a binary image. Two-step noise removal was employed after the creation of binary water body and land classes. In the first step, the largest white pixel blob in the binary image was automatically selected and the white blobs that were smaller than the largest blob are set as black. In the second step, the gap-filling process (Soille, 1999) was performed for cleaning the small black pixels within the white pixel groups.

The final binary results by exploiting SVM and RF are given in Figure 4a) and b). The generated shorelines are given in Figure 4c) and d).

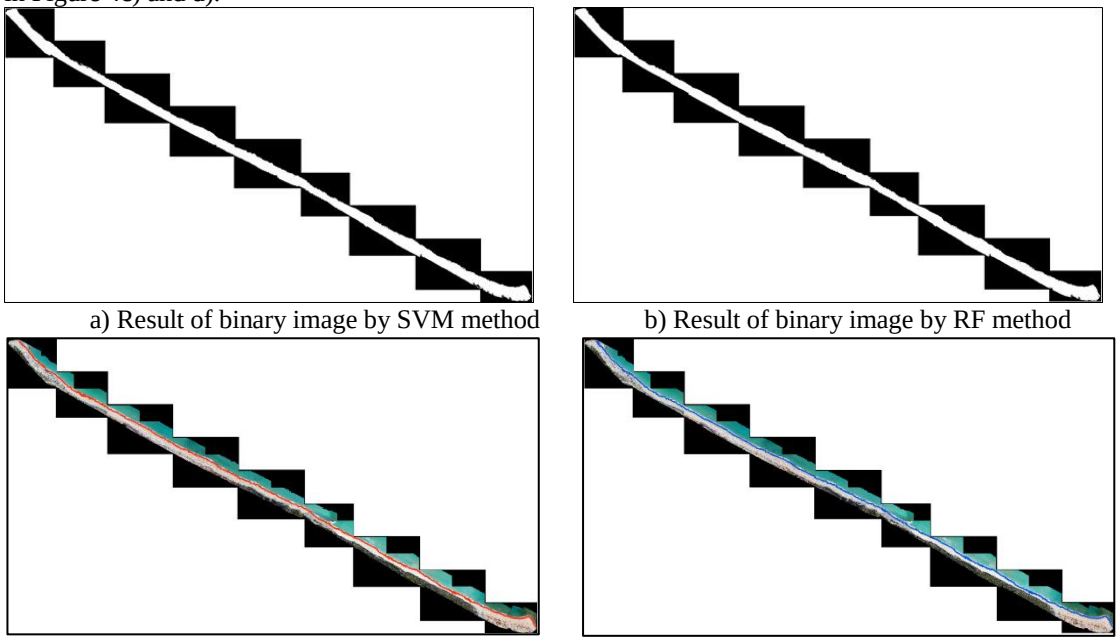

a) Result of binary image by SVM method b) Result of binary image by RF method

c) Obtained shoreline by SVM method d) Obtained shoreline by RF method

Figure 4 Obtained shorelines by SVM and RF methods

The DSAS tool was utilized for accuracy assessment (Thieler et al., 2009). For this purpose, the GNSS measurements were taken as reference data and compared with obtained shorelines from both the SVM and RF methods. This study employed the Net Shoreline Movement (NSM) of the DSAS, which measures perpendicular distances between reference and source shorelines using transects. The length of transects was selected as 100 m in 1 m intervals.

The calculated mean and root mean square errors of the perpendicular distances between the reference and the derived shorelines for both the SVM and RF methods are shown in Table 3. As can be seen in Table 3, similar results have been created from both methods.

Table 3 Accuracy assessment results

Method	Average Error (m)	RMS Error (m)
SVM	0.935	1.708
RF	0.939	1.727

The classified differences and resulted ratios are given in Figure 6. The differences of 71.86% and 71.61% are in the 0–1 m interval for SVM and RF, respectively. According to Figure 7, the performances of both methods are almost identical. The general structure of the graphics is also quite similar. Since flight permission was valid only for 20 September 2017, the UAV flight had to be carried out in the wavy season. According to the European Centre for Medium-Range Weather Forecasts (ECMWF) ERA-Interim database (ECMWF, 2019), the wind speed and direction for the study area on the flight date were 9.403114 (m/s) and SE, respectively. The GNSS measurements were completed in six hours, which caused a time difference with the flights.

The results indicate that seasonal and timewise planning of flights plays a key role for end product quality. For example, according to the ECMWF data, the calmest season for our study area is in the middle of October due to

active south winds (ECMWF, 2019). However, it was not possible to perform new flights at this time due to the bureaucratic flight permission process. In this study, the tide effects have not been considered, since we did not aim at temporal change detection.

We planned to collect training samples from one patch and implement the SVM and RF methods on the other patches. Due to unbalanced colour effects in the created digital orthophoto, a patch-wise training sample collection strategy was applied. The number of selected training samples for each class was around 0.001%.

Consequently, it has been proved that the proposed framework is able to create satisfactory, accurate shorelines in our study area. The obtained results show that mean shoreline extraction accuracy of both methods is around 1 m. This indicates that the shorelines can be extracted in a 1 m buffer by using our proposed framework even in the wavy season.

5. CONCLUSIONS

The UAV can be regarded as promising and reliable technology for coastal-related studies. In this study, the SVM and RF methods were tested and the results show that these methods are capable of being used for shoreline extraction and can be implemented on a UAV-derived digital orthophoto. Our results indicate that UAV-based monitoring of coastal areas has undeniable potential due to its high accuracy, mobility and cost-effectiveness. The resolution of mounted IMU and GPS systems was not sufficient to obtain exterior orientation parameters of images; therefore, in this study, additional ground control point measurements were required. However, the IMU and GPS precision of new-generation UAV systems in the market are sufficient for these kinds of tasks.

In general, UAVs deserve to be taken into account for shoreline extraction studies due to the advantages that have been observed in this study. Another important factor is that the results have been obtained from an RGB camera. If the developments of UAV cameras are taken into consideration, the use of multispectral cameras, which include near infrared band, may increase the accuracy of shoreline extraction.

Although the SVM and RF methods have been used in various studies for image classification purposes, they have not been utilized for shoreline extraction. This study shows that these two machine-learning methods also provide remarkable results for this purpose. The proposed framework can be used to create an essential data source for many coastal-related studies such as monitoring, determining temporal changes and modelling sediment transport.

Acknowledgments

This study has been supported by TUBITAK (The Scientific and Technological Research Council of Turkey), project number 115Y718.

References

Bayram B., Avsar O., Seker D. Z., Kayı A., Erdogan M., Eker O., Janpaule I., Reis H. C. 2017. The Role of National and International Geospatial Data Sources in Coastal Zone Management, Fresenius Environmental Bulletin, Volume 26, No. 1/2017, pages 383-391.

Belgiu M. and Drăguţ L. 2016. Random forest in remote sensing: A review of applications and future directions,"ISPRS J. Photogramm. Remote Sens., vol. 114, pp. 24–31.

Breiman L. 2001. Random Forests, Mach. Learn., vol. 45, no. 1, pp. 5–32.

Casella E., Rovere A., Pedroncini A. , Mucerino L. , Casella M. , Cusati L. A. O., Vacchi M., Ferrari M., Firpo M. 2014. Study of wave runup using numerical models and low-altitude aerial photogrammetry: A tool for coastal management, Estuarine, Coastal and Shelf Science 149,160-167.

Čermáková I., Komárková J., Sedlák P. 2016. Using UAV to Detect Shoreline Changes: Case Study – Pohranov Pond, Czech Republic, The International Archives of the Photogrammetry, Remote Sensing and Spatial Information Sciences, Volume XLI-B1, 2016 XXIII ISPRS Congress, 12–19 July 2016, Prague, Czech Republic, p.803-808, doi:10.5194/isprsarchives-XLI-B1-803-2016.

Clapuyt F., Vanacker V., Oost K. V. 2016. Reproducibility of UAV-based earth topography reconstructions based

on Structure-from-Motion algorithms, Geomorphology 260, 4–15.

Dellaert F., Seitz S.M., Thorpe C.E. Thrun S. 2000. Structure from motion without correspondence, Computer Vision and Pattern Recognition, 2000. Proceedings. IEEE Conference on 15-15 June 2000, DOI: 10.1109/CVPR.2000.854916.

Demir N., Bayram B., Seker D. Z., Oy S., Bozkurt S., Ince A. 2019. Analysing the impact of an earthquake on the shoreline using SAR images as alternative dataset, Fresenius Environmental Bulletin, Volume 28, No. 2/2019 pages 516-522.

Demir N., Oy S. , Erdem F. , Seker D. Z. , Bayram B. 2017. Integrated Shoreline Extraction Approach With Use of Rasat MS And Sentinel-1A SAR Images, ISPRS Annals of the Photogrammetry, Remote Sensing and Spatial Information Sciences, Volume IV-2/W4, 2017 ISPRS Geospatial Week 2017, 18–22 September 2017, Wuhan, China, p.445-449, https://doi.org/10.5194/isprs-annals-IV-2-W4-445-2017.

ECMWF. 2019. European Centre for Medium-Range Weather Forecasts, Retrieved April 04, 2019, from https://www.ecmwf.int/

Flener C, Vaaja M, Jaakkola A, Krooks A, Kaartinen H, Kukko A, et al. 2013. Seamless mapping of river channels at high resolution using mobile LIDAR and UAV-photography. Remote Sensing 5(12):6382–407. http://doi.org/10.3390/rs5126382.

Ghamisi P., Plaza J., Chen Y., Li J., and Plaza A. 2017. Advanced Supervised Spectral Classifiers for Hyperspectral Images: A Review, IEEE Geosci. Remote Sens. Mag., vol. 5, no. 1, pp. 8–32.

Gislason P. O., Benediktsson J. A., and Sveinsson J. R. 2006 .Random Forests for land cover classification, Pattern Recognit. Lett., vol. 27, no. 4, pp. 294–300, Mar. 2006.

Gomez, C., Hayakawa, Y., Obanawa, H. 2015. A study of Japanese landscapes using structure from motion derived DSMs and DEMs based on historical aerial photographs: new opportunities for vegetation monitoring and diachronic geomorphology. Geomorphology 242, 11–20.

Gu Y., Liu T., Jia X., Benediktsson J. A., and Chanussot J. 2016. Nonlinear Multiple Kernel Learning with Multiple-Structure-Element Extended Morphological Profiles for Hyperspectral Image Classification, IEEE Trans. Geosci. Remote Sens., vol. 54, no. 6, pp. 3235–3247, 2016.

Guillot B., Musereau J., Dalaine B., Morel J. 2018. Coastal Dunes Mobility Integration and Characterization: Developing of a Flexible Volume Computing Method, Journal of Geographic Information System, 10, 503-520.

Han J., Kamber M., Pei J. 2011. Data Mining – Concepts & Techniques, 3rd ed. Morgan Kaufmann Publishers, ISBN 978-0-12-381479-1.

Haykin S. 2009. Neural Networks and Learning Machines, 3rd ed. Pearson Prentice Hall.

Jamil, A. 2018. Tree Species Classificatioin Ffrom High Resolution Digital Orthophoto Maps, Yildiz Technical University, Graduate School of Science And Engineering, Doctoral Thesis.

Kalke H., Loewen M. 2018. Support vector machine learning applied to digital images of river ice conditions, Cold Regions Science and Technology 155, 225–236.

Lim M., Dunning S. A., Burke M., King H., King N. 2015. Quantification and implications of change in organic carbon bearing coastal dune cliffs: A multiscale analysis from the Northumberland coast, UK, Remote Sensing of Environment 163 1–12.

Liu Q. , Trinder J., Turner I. 2016. A Comparison of Sub-Pixel Mapping Methods for Coastal Areas, ISPRS Annals of the Photogrammetry, Remote Sensing and Spatial Information Sciences, Volume III-7, 2016, XXIII ISPRS Congress, 12–19 July 2016, Prague, Czech Republic, p.67-74, doi:10.5194/isprsannals-III-7-67-2016

Mallast U. and Siebert C. 2019. Combining continuous spatial and temporal scales for SGD investigations using UAV-based thermal infrared measurements, Hydrol. Earth Syst. Sci., 23, 1375–1392, 2019.

https://doi.org/10.5194/hess-23-1375-2019.

Mancini F., Dubbini M., Gattelli M., Stecchi F., Fabbri S., Gabbianelli G. 2013, Using Unmanned Aerial Vehicles (UAV) for High-Resolution Reconstruction of Topography: The Structure from Motion Approach on Coastal Environments, Remote Sens., 5, 6880-6898; doi:10.3390/rs5126880.

Milas A. S., Arend K., Mayer C., Simonson M. A. and Mackey S. 2018. Different colours of shadows: classification of UAV images, International Journal of Remote Sensing, Vol. 38, Nos. 8–10, 3084–3100. http://dx.doi.org/10.1080/01431161.2016.1274449.

Mišijovský, J., Michalková, M. Š., Petyniak, O., Máčka, Z., Trizna, M. 2015. Spatiotemporal evolution of a unique preserved meandering system in Central Europe — The Morava River near Litovel, Catena, 127, 300–311.

Murtiyoso A., Pierre G. 2017. Documentation of Heritage Buildings Using Close-Range UAV Images: Dense Matching Issues, Comparison and Case Studies. The Photogrammetric Record 32(159): 206–229 (September 2017), DOI: 10.1111/phor.12197, p. 207-229.

Nagarajan S., Khamaru S. , De Witt P. 2019. UAS based 3D shoreline change detection of Jupiter Inlet Lighthouse ONA after Hurricane Irma, Journal of Remote Sensing, DOI: 10.1080/01431161.2019.1569792.

Nolet C., van Puijenbroek M., Suomalainen J., Limpens J., Riksen M. 2018. UAV-imaging to model growth response of marram grass to sand burial: Implications for coastal dune development, Aeolian Research, 31. 50-61.

Oleire-Oltmanns, S., Marzolff, I., Peter, K. D., & Ries, J. B. 2012. Unmanned aerial vehicle (UAV) for monitoring soil erosion in Morocco. Remote Sensing, 4, 3390–3416. http://dx.doi.org/10.3390/rs4113390.

Pix4d, 2017 Retrieved December, 12, 2018 from https://pix4d.com/

Rusnák M., Sládeka J., Kidováa A., Lehotskýa M. 2018. Template for high-resolution river landscape mapping using UAV technology, Measurement 115,139–151.

Scarelli F. M., Sistilli F., Fabbri S., Cantelli L., Barboza Eduardo G., Gabbianelli G. 2017. Seasonal dune and beach monitoring using photogrammetry from UAV surveys to apply in the ICZM on the Ravenna coast (Emilia-Romagna, Italy), Remote Sensing Applications: Society and Environment, Volume 7, Pages 27-39.

Soille, P. 1999. Morphological Image Analysis: Principles and Applications, Springer-Verlag, pp. 173-174.

Talavera L., Del Río L., Benavente J., Barbero L. and López-Ramírez J. A. 2018. UAS as tools for rapid detection of storm-induced morphodynamic changes at Camposoto beach, SW Spain, International Journal of Remote Sensing, Vol. 39, No. 15–16, 5550–5567. https://doi.org/10.1080/01431161.2018.1471549.

Thieler, E. R., Himmelstoss, E.A., Zichichi, J.L., Ergul, A. 2009. Digital Shoreline Analysis System (DSAS) version 4.0 -An ArcGIS extension for calculating shoreline change. U.S. Geological Survey, Open-File Report 2008-1278.

Ullman, S., 1979. The interpretation of structure from motion. Proc. R. Soc. Lond. Ser. B 203, 405–426.

Vapnik V. N. 1995. The Nature of Statistical Learning Theory. Springer, N.Y., ISBN 0-387-94559-8.

Vapnik V. N. 1999. An Overview of Statistical Learning Theory, IEEE Transactions on Neural Networks, Vol. 10, N0. 5, p. 988-999.

Xia H., Zhao W., Li A. , Bian J. and Zhang Z. 2018. Subpixel Inundation Mapping Using Landsat-8 OLI and UAV Data for a Wetland Region on the Zoige Plateau, China, Remote Sens., 9, 31; doi:10.3390/rs9010031.

Zaitoun N., M., Aqel M., J. 2015. Survey on Image Segmentation Techniques, Procedia Computer Science 65 797 – 806.